Optimal Control Strategy With Efficiency and Reliability Improvement for Offshore DC Microgrids

Xiangchen Zhu, *Student Member, IEEE*, Pengxiang Huang, *Member, IEEE*, Hanwen Zhang, *Graduate Student Member, IEEE*, Yanbo Wang, *Senior Member, IEEE*, Ruizhi Wei, *Graduate Student Member, IEEE*, Ning Wang, *Student Member, IEEE*, Yunwei Li, *Fellow, IEEE*, and Zhe Chen, *Fellow, IEEE*

***Abstract*—Offshore microgrids, due to their remote location and lack of external energy support, face significant challenges in wide-range load operation and maintenance. Consequently, efficiency and reliability are critical concerns for converters in offshore dc microgrids. This article presents an optimal control strategy aimed at enhancing both efficiency and reliability. A normalized nonlinear relationship between power loss and thermal stress of a paralleled converter is first established. Based on this, a dual-objective optimization function with an active weight function as well as a system overall performance index is established. The active weight function dynamically adjusts the control priority based on converter efficiency and switching device thermal stress. Then, the optimal power-sharing strategy is derived by the Lagrange multiplier method with the proposed optimal function. Additionally, to accommodate a wide load range, an optimal selection strategy for operating converter combinations is proposed, requiring only low-bandwidth communication. Experiment verification is given to validate the effectiveness of the proposed control strategy. The experiment results demonstrate that the proposed control strategy can improve the overall performance of offshore microgrids by optimizing efficiency and reliability.**

***Index Terms*—Efficiency, offshore dc microgrids, optimal operation, paralleled converters, thermal stress.**

I. Introduction

THE exploitation of offshore renewable energies, such as offshore wind energy, Photovoltaic (PV), wave energy, and tidal energy, etc. [1], [2], is an important trend throughout the world. Offshore dc microgrid is a promising solution to utilize offshore renewable energies in an efficient and cost-effective way because it can realize energy production and consumption within offshore environments [3], [4], [5], [6]. A typical dc microgrid consists of multiple paralleled distributed generators (DGs) by dc–dc converter to dc bus [7], [8], [9].

In practical operation, different DG converters may have different operating characteristics, including design margin, aging levels, and lifetime. [10], [11]. This inevitably leads to differences in efficiency among converters operating under the same load condition [10]. In addition, during long-term operation, converters with different aging levels can increase converter fault risk, which further impacts system reliability [12], [13]. Meanwhile, the maintenance of offshore dc microgrids is usually time-consuming and expensive. As a result, the efficiency and reliability of offshore microgrids with multiple paralleled dc converters emerge as two key indices of concern.

Due to the fluctuation of renewable energies, the paralleled converters in offshore dc microgrids are operated under a wide load range, which may reduce system efficiency under light load conditions [14], [15]. Bartal and Nagy [16] employed Game theory to improve paralleled converter-dominated power system efficiency in a wide load range, including both heavy load and light load conditions. In [17], a data-driven control with model-free adaptive control and dual-droop control is proposed to improve converter efficiency in microgrids in light load conditions. A hierarchical control framework with a finite state machine as a secondary control to improve the efficiency of a paralleled converter is proposed in [14] and [18]. However, the efficiency characteristics of different converters have been given limited consideration in the studies. To address it, several research efforts have been performed to improve system efficiency by considering different efficiency characteristics of paralleled converters. A quadratic loss model is used to represent converter power loss and efficiency characteristics in [19]. A power-sharing strategy with virtual impedance-based droop control is developed in [20] and [21], which effectively optimizes power-sharing between microgrids to improve system performance. To adjust power-sharing in a high-efficiency way, efficiency-prioritized droop control for the paralleled converters is developed in [22]. However, the efficiency-prioritized control may lead to unbalanced thermal stress on converters and further influence converter reliability.

Received 18 March 2025; accepted 24 June 2025. Date of publication 1 July 2025; date of current version 27 August 2025. Recommended for publication by Associate Editor M. ElMoursi. *(Corresponding author: Yanbo Wang.)*

Xiangchen Zhu, Yanbo Wang, Ning Wang, and Zhe Chen are with the Energy Department, Aalborg University, Aalborg 9220, Denmark (e-mail: ywa@et.aau.dk).

Pengxiang Huang is with the National Renewable Energy Laboratory, Golden 80402 USA.

Hanwen Zhang is with the Department of Electronic and Electrical Engineering, University of Bath, Bath BA2 7AY, UK.

Ruizhi Wei and Yunwei Li are with the Department of Electrical and Computer Engineering, University of Alberta, T6G 2R3, Canada.

Color versions of one or more figures in this article are available at https://doi.org/10.1109/TPEL.2025.3585117.

Digital Object Identifier 10.1109/TPEL.2025.3585117

In addition to efficiency, reliability is another crucial metric for dc microgrids, particularly in practical implementations deployed in remote areas to support critical loads. Offshore dc microgrids are typically located in remote areas and with long maintenance cycles, which makes timely repairs of equipment failures challenging. Therefore, it is necessary to improve the reliability of converters in an offshore dc microgrid. Currently, research on the operation of converters considering reliability has gained significant attention, particularly in applications such as smart transformers and wind power. [23], [24]. For example, to reduce the high maintenance cost for smart transformers, a lifetime-based power-sharing strategy with reliability improvement is proposed in [13]. Buticchi et al. [25] applied a similar control strategy on a quadruple active bridge dc–dc converter, whereas Marquez et al. [26] adapted an accumulated damage-based control in a dc–dc boost converter. Note that research in [23], [24], [25], and [26] consider accumulated damage as a control parameter. Previous efforts have intended to improve converter reliability with the quantification of converter accumulated damage. The accumulated damage can also be addressed as the remaining useful lifetime. Power sharing for modular power converters in electric aircraft based on remaining useful lifetime is proposed in [27]. However, the accumulated damage value is calculated by accumulating the working conditions of the converter throughout its entire life cycle, where the errors of the calculated accumulated damage value are inevitable. The introduction of accumulated damage, which is an imprecise parameter, into the control loop may decrease system reliability.

The junction temperature of switching devices is a critical factor affecting reliability [28], [29]. The switching device number to the failure times lifetime model is discussed comprehensively in [30]. Each type of lifetime model in [30] illustrates the impact of junction temperature on switching device failure. In that case, balancing thermal stress among switching devices can effectively enhance system reliability [31], [32]. In [33] and [34], active thermal management by junction temperature balance control for paralleled converters is developed to enhance system reliability. However, the above-mentioned thermal analysis and lifetime evaluation slightly consider the effects of converter control loops. In [35], the junction temperature is adopted as a variable in control loops. However, it mainly considers thermal stress under extreme conditions. The improvement in converter efficiency enhances its reliability and extends its operational lifespan. However, the optimal operation points of efficiency and reliability improvement are not identical. The research work performed in [36] suggests that reduced thermal stress may increase extra power loss, and the efficiency improvement comes at the cost of reduced system reliability. Thus, the optimal operation of offshore dc microgrid converters considering both efficiency and reliability needs to be explored further.

In our previous work, a hierarchical control framework was proposed to improve the efficiency and reduce operational costs of offshore dc microgrids [14]. Nevertheless, system reliability was not addressed in that work. This issue is particularly critical for offshore dc microgrids, where both efficiency and reliability demand careful consideration. Therefore, this article presents an optimal operation strategy to enhance both efficiency and reliability of paralleled converters in offshore microgrids. The main contributions of this work are clarified as follows:

1) With consideration of both efficiency and reliability requirements of the converter, a dual-objective optimal model and overall system performance index are established.
2) An active dual-objective optimal weight function that can prioritize the efficiency in light load and prioritize the thermal stress in heavy load is established. Based on that, the optimal power-sharing strategy considering both efficiency and reliability in a wide load range is developed.
3) A decentralized optimal selection strategy is proposed for operating converter combinations under a wide load range, which is optimized based on the established system's overall performance index.

The rest of this article is organized as follows. In Section II, a normalized nonlinear model of efficiency and switching device thermal stress is established to estimate system operation performance. In Section III, an optimal power-sharing strategy among paralleled converters with a Lagrange mutiobjective optimization function is proposed. Furthermore, the optimal selection strategy for operating converter combinations is proposed to improve system performance in a wide load range. The effectiveness of the proposed control strategy with different cases is validated through experiments in Sections IV and V. Finally, Section VI concludes this article.

II. System Modeling

This work takes an offshore dc microgrid as the application with renewable energy sources, including wind power, wave energy, solar power, and loads like electrolyzers.

A. Efficiency Modeling

The efficiency of *n*-paralleled converters can be represented by the modeling of the converter's total loss. The converter power loss $P_{\text{loss\_con\_}i}$ can be represented as

$$P_{\text{loss\_}i} = a_i i_{\text{o}i}^2 + b_i i_{\text{o}i} + c_i \tag{1}$$

where $i_{\text{o}i}$is the output current of the *i*th converter. a_i, b_i, and $c_i$are the power loss coefficients, which can be obtained by fitting efficiency–output power curves [15], [19]. The efficiency–output current curve can be obtained by fitting the test results of the converter power loss across various load conditions. The total power loss from DGs includes converter power and cable network power loss. The total power loss of the *i*th DG $P_{\text{loss\_}i}$ can be represented as

$$P_{\text{loss\_}i} = (a_i + R_{\text{line\_}i})\, i_{\text{o}i}^2 + b_i i_{\text{o}i} + c_i \tag{2}$$

where $R_{\text{line\_}i}$ is the corresponding cable resistance of the *i*th DG. $V_{\text{o}i}$ is the output voltage of the *i*th converter.

The system's total loss $P_{\text{loss\_sys}}$ can be represented as

$$P_{\text{loss\_sys}} = \sum_{i=1}^{N} P_{\text{loss\_}i}. \tag{3}$$

B. Switching Device Power Loss Modeling

The switching device's power loss can be represented as

$$P_{\text{loss\_SD}} = P_{\text{loss\_SD\_cond}} + P_{\text{loss\_SD\_switch}} \tag{4}$$

where $P_{\text{loss\_SD}}$ is the total power loss on the switching device, $P_{\text{loss\_SD\_cond}}$ is the conduct loss on the switching device, and$P_{\text{loss_SD_switch}}$ is the switching loss on the switching device.

The conduction loss of the switching device can be represented as

$$P_{\text{loss\_SD\_cond}} = V_{\text{CEsat}} \cdot D \cdot i_C \tag{5}$$

where V_{CEsat} is collector-emitter saturation voltage, D is duty cycle, and i_C is collector current.

In the operation of switching devices, the value of the collector–emitter saturation voltage changes in response to variations in the collector current. Accordingly, the value of collector–emitter saturation voltage, considering the switch device current load, can be represented as

$$V_{\text{CEsat}} = V_{\text{CEsat\_0}} + \psi \cdot i_C \tag{6}$$

where $V_{\text{CEsat\_0}}$ is the initial value of the collector–emitter saturation voltage. The coefficient ψ can be obtained from the datasheet [38], [39], [40], [41].

The switching loss can be represented as

$$\begin{aligned} P_{\text{loss\_SD\_switch}} &= f_{\text{switch}} \cdot E_{\text{switch}} \\ E_{\text{switch}} &= \frac{1}{2} V_{\text{SW}} \cdot D \cdot i_C \left(t_{\text{ON}} + t_{\text{OFF}}\right) \end{aligned} \tag{7}$$

where f_{switch} is switching frequency, E_{switch} is switching energy loss, V_{SW} is the voltage across the switch when it is in the process of turning ON or OFF, t_{ON} is the time duration for the switch turning ON, and t_{ON} is the time duration for the switch turning OFF.

Taking the boost converter in continuous current mode as an example, the relationship between the converter's output current and the switch device's collector current is given as

$$i_{\text{o}} = \frac{D}{(1-D)} i_C. \tag{8}$$

Combining (4), (5), (6), and (8), the power loss of the switching device can be represented as

$$\begin{aligned} P_{\text{loss\_SD}} = {} & \psi \frac{(1-D)^2}{D} {i_{\text{o}}}^2 \\ & + \left[V_{\text{CEsat\_0}} + \frac{1}{2} f_{\text{switch}} V_{\text{SW}} \left(t_{\text{ON}} + t_{\text{OFF}}\right) \right] (1-D)\, i_{\text{o}}. \end{aligned} \tag{9}$$

C. Electrical Thermal Modeling

The junction temperature of the switching device can be estimated by an electrical thermal model without direct measurements, which is easy to adopt in practical operation. The equivalent thermal model shown in Fig. 1 is applied to estimate junction temperature with power loss on the switching device.

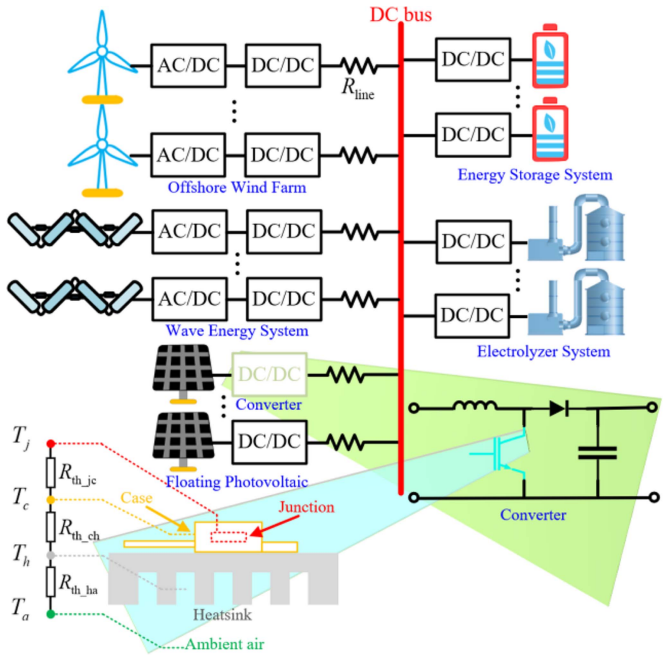

Fig. 1. Diagram of offshore microgrid system and the equivalent thermal model of the switching device.

The junction temperature of the switching device can be expressed as

$$T_j = \left(R_{\text{th\_jc}} + R_{\text{th\_ch}} + R_{\text{th\_ha}}\right) \cdot P_{\text{loss\_SD}} + T_{\text{a}} \tag{10}$$

where T_{j} and T_{a} are the temperature of the junction and ambient. The thermal resistances in the equivalent thermal model are provided by the datasheet. $R_{\text{th\_jc}}$ is the thermal resistance between junction and case. $R_{\text{th\_ch}}$ is the thermal resistance between case and heatsink. $R_{\text{th\_ha}}$ is the thermal resistance between the case and the ambient temperature.

D. Converter Reliability Modeling

The Coffin–Manson model represents the relationship between switching device junction temperature and lifetime [30] given as

$$N_f = 302500 \left[\frac{1}{{\Delta T_j}^{5.039}} \exp\left(\frac{9.891 \times 10^{-20}}{k_{\text{B}} T_{\text{j\_mean}}} \right) \right] \tag{11}$$

where N_f is the number of cycles of failure. k_{B} is the Boltzmann constant. ΔT_j expresses thermal cycling. $T_{\text{j\_mean}}$ expresses thermal stress on the switching device.

Bayerer's lifetime model is known as the most comprehensive analytical lifetime model [30], given as

$$N_f = K {\Delta T_j}^{\beta_1} \exp\left(\frac{\beta_2}{T_{\text{j\_mean}} + 273K} \right) \cdot {t_{\text{ON}}}^{\beta_3} \cdot {i}^{\beta_4} \cdot {V}^{\beta_5} \cdot {D}^{\beta_6} \tag{12}$$

where K and β_1 to β_6 are constants extracted from the switching device reliability test.

Both Coffin–Manson and Bayerer lifetime models reveal the relationship between the junction temperature of switching devices and their reliability. The switching device operating under high thermal stress exhibits a reduced number of failure

cycles. Therefore, mitigating extreme thermal stress on switching devices within the system can significantly improve overall reliability.

Different thermal stresses on the switching device led to different aging levels, which can be represented by accumulated damage under different operating conditions. The converter's accumulated damage can be expressed as

$$\mathrm{AD} = \sum_{\mathrm{LP}\_i=1}^{n} \frac{N_{\mathrm{LP}\_i}}{N_f\left(\mathrm{LP}\_i\right)} \tag{13}$$

where LP_i is the different load profile and N_{LP_i} is the switch device operation numbers under the ith load profile.

E. Proposed Optimization Model

For the converter with multiple switching devices or converters connected in series within the same branch, the switching device handling the highest thermal stress can be considered as an indicator of the converter to indicate the overall thermal stress condition. The representative thermal stress of the ith converter with n switching devices can be expressed as

$$R_{\mathrm{th}\_i} \cdot P_{\mathrm{loss\_SD}\_i} = \max \begin{pmatrix} R_{\mathrm{th}\_i\_1} \cdot P_{\mathrm{loss\_SD}\_i\_1}, \\ R_{\mathrm{th}\_i\_2} \cdot P_{\mathrm{loss\_SD}\_i\_2} \cdots \\ R_{\mathrm{th}\_i\_n} \cdot P_{\mathrm{loss\_SD}\_i\_n} \end{pmatrix}. \tag{14}$$

The efficiency of paralleled converters is optimal when the power loss of the converter is minimized. Meanwhile, the switching device junction temperature is related to the power loss in the switching device. To achieve efficient operation while accounting for thermal stress, a multiobjective optimization function is proposed consisting of the following steps. First, normalize the nonlinear relationship of P_{loss_i}, $P_{\mathrm{loss\_SD}\_i}$, and i_{oi}, respectively. Then, combining the normalized P_{loss_i} and $P_{\mathrm{loss\_PD}\_i}$ with weight coefficients A_i and B_i. The mutiobjective optimization function is established as

$$S_i = A_i \frac{P_{\mathrm{loss}\_i}}{P_{\mathrm{loss\_rated}}} + B_i \frac{R_{\mathrm{th}\_i} \cdot P_{\mathrm{loss\_SD}\_i}}{R_{\mathrm{th\_rated}} \cdot P_{\mathrm{loss\_SD\_rated}}} \tag{15}$$

where

$$\begin{cases} P_{\mathrm{loss\_rated}} = \sum_{i=1}^{n} P_{\mathrm{loss}\_i\_\mathrm{rated}} = \sum_{i=1}^{n} P_{\mathrm{loss}\_i}\big|_{i_{oi\_\mathrm{rated}}} \\ P_{\mathrm{loss\_SD\_rated}} = \sum_{i=1}^{n} P_{\mathrm{loss\_SD}\_i\_\mathrm{rated}} = \sum_{i=1}^{n} P_{\mathrm{loss\_SD}\_i}\big|_{i_{oi\_\mathrm{rated}}} \\ R_{\mathrm{th}\_i} = R_{\mathrm{th\_jc}\_i} + R_{\mathrm{th\_ch}\_i} + R_{\mathrm{th\_ha}\_i}, R_{\mathrm{th\_rated}} = \sum_{i=1}^{n} R_{\mathrm{th}\_i} \\ 0 \le A_i \le 1, 0 \le B_i \le 1, A_i + B_i = 1 \end{cases}.$$

By combining (2) and (13), it can be derived as

$$S_i = a_i^* i_{oi}^2 + b_i^* i_{oi} + c_i^* \tag{16}$$

$$\begin{cases} a_i^* = \frac{A_i a_i + A_i R_{\mathrm{line}\_i}}{P_{\mathrm{loss\_rated}}} + \frac{B_i \cdot R_{\mathrm{th}\_i} \cdot \psi \frac{(1-D)^2}{D}}{R_{\mathrm{th\_rated}} \cdot P_{\mathrm{loss\_SD\_rated}}} \\ b_i^* = \frac{A_i b_i}{P_{\mathrm{loss\_rated}}} \\ \quad + \frac{B_i \cdot R_{\mathrm{th}\_i}\left[V_{\mathrm{CEsat\_0}} + \frac{1}{2} f_{\mathrm{switch}} V_{\mathrm{SW}}(t_{\mathrm{ON}} + t_{\mathrm{OFF}})\right](1-D)}{R_{\mathrm{th\_rated}} \cdot P_{\mathrm{loss\_SD\_rated}}} \\ c_i^* = \frac{A_i c_i}{P_{\mathrm{loss\_rated}}} \end{cases}$$

where A_i is the weight coefficient for power loss and B_i is the weight coefficient for power loss in switching devices, which indicates junction temperature and reliability. $P_{\mathrm{loss\_rated}}$ and $P_{\mathrm{loss\_SD\_rated}}$ are the power loss of the converter and switching device in rated load conditions.

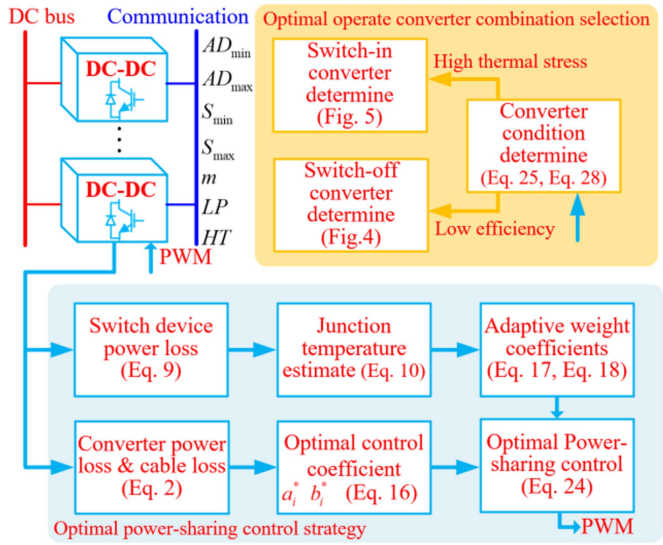

Fig. 2. Proposed optimal control strategy framework.

The weight coefficients for efficiency and junction temperature should be adaptively adjusted based on the junction temperature of the switching device. When the switching device junction temperature is below 60 °C, the switching device handles low thermal stress. In this scenario, the weighting coefficients are set to $A_i = 1$ and $B_i = 0$, enabling the system to achieve higher efficiency. When the junction temperature is between 60 °C and 90 °C, the multiobjective weight coefficients are adaptively modified to optimize both converter efficiency and component thermal stress. For junction temperature exceeding 90 °C, the weight coefficients are set to $A_i = 0$ and $B_i = 1$, effectively managing thermal stress distribution among parallel converters, to enhance system reliability.

By using the sigmoid function, the proposed thermal stress weight coefficient B_i can be expressed as

$$B_i = \begin{cases} 0 & (T_j \le 30) \\ 1/\left(1 + e^{-0.08(T_j - 60)}\right) & (30 < T_j \le 90) \\ 1 & (T_j < 90) \end{cases}. \tag{17}$$

The converter efficiency weight coefficient A_i can be expressed as

$$A_i = 1 - B_i. \tag{18}$$

III. Proposed Optimal Control Strategy

Fig. 2 shows the diagram of the proposed optimal control strategy, which includes two parts. Part 1 is optimal power sharing between paralleled converters considering efficiency and reliability. Part 2 is the optimal selection strategy for operating converter combinations, which contributes to system efficiency and reliability in a wide load range.

The dual-objective optimal power-sharing strategy is introduced to determine the optimal power-sharing ratio among paralleled converters adaptively according to the features of

individual converter efficiency, converter corresponding cable resistance, and converter electrical-thermal characteristics. The proposed strategy can improve system efficiency and reliability. The optimal selection strategy for operating converter combinations is used to deal with the wide load range. The control system will enable the most suitable converter to switch ON/OFF according to the system load conditions, converter thermal stress, and accumulated damage. The proposed strategy can improve system efficiency and avoid switching device operation under high thermal stress. The details of the proposed optimal control strategy are given in the following sections.

A. Optimal Power-Sharing: Efficiency Improvement and Switching Device Thermal Stress-Sharing

To optimize the power-sharing ratio of paralleled converters, the Lagrange function is established with the Lagrange multiplier as

$$L = \sum_{i=1}^{n} S_i + \lambda \left(i_{\text{Load}} - \sum_{i=1}^{n} i_{\text{o}i} \right) \tag{19}$$

$$\text{s.t.} \sum_{i=1}^{n} i_{\text{o}i} = i_{\text{Load}}.$$

The necessary condition of the Lagrange function is

$$\left\{ \frac{\partial S_1}{\partial i_{\text{o}1}} = \frac{\partial S_2}{\partial i_{\text{o}2}} = \cdots = \frac{\partial S_n}{\partial i_{\text{o}n}}. \right. \tag{20}$$

According to the Lagrange optimization result, the optimal power-sharing ratio of paralleled converters with high efficiency and reliability is given as

$$2a_i^* i_{\text{o}i} + b_i^* = 2a_j^* i_{\text{o}j} + b_j^* = \ldots = 2a_n^* i_{\text{o}n} + b_n^*. \tag{21}$$

Take the Lagrange optimization results as the target for power-sharing ratios among paralleled converters. The droop control-based optimal power-sharing considering efficiency and reliability for an n-paralleled converter is

$$V_i^* = V_{i\_\text{ref}} - 2a_i^* i_{\text{o}i} - b_i^*. \tag{22}$$

To deal with the influence of the converter corresponding cable resistance, the power-sharing control considering the cable resistance is established as

$$V_i^* = V_{i\_\text{ref}} + \left(R_{\text{line}i} - 2a_i^* \right) i_{\text{o}i} - b_i^*. \tag{23}$$

The droop control and cable resistance will decrease the bus voltage. In an islanded power system, the converter should maintain the bus voltage. The proposed grid-forming optimal power-sharing control is given as

$$\begin{aligned} V_i^* &= V_{i\_\text{ref}} + \left(R_{\text{line}i} - 2a_i^* \right) i_{\text{o}i} - b_i^* + \Delta V \\ \Delta V &= \frac{1}{n-1} \sum_{\substack{j=1 \\ j \neq i}}^{n} \left(R_{\text{line}j} - 2a_j^* \right) i_{\text{o}j} - b_j^*. \end{aligned} \tag{24}$$

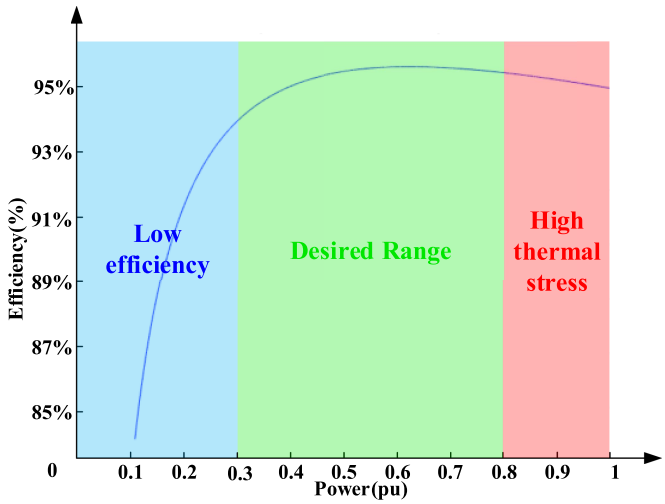

Fig. 3. Optimal control priority under different load conditions.

B. Active Operate Converter Combination Selection According to Load Condition and Thermal Stress

The offshore dc microgrid converters operate within a wide load range. The efficiency of the converter changes with variations in load conditions. The number of paralleled converters will affect the efficiency. The paralleled converter efficiency can be decreased significantly when the converter load is lower than 30% . Meanwhile, the converter's thermal stress will be higher with heavy loads. In that case, the proposed optimal selection strategy for operating converter combinations is introduced to keep each converter operation in a desired range as shown in Fig. 3.

When the load decreases, the converter that needs to be switched OFF can be selected by considering the following three aspects.

1) Improve system efficiency.
2) Avoid high accumulated damage on certain converters.
3) Choose the one that can improve system efficiency as well as thermal performance after it is switched OFF with the help of the system's overall performance index S.

Defining LP = 1 to indicate the converter under the light load condition as shown in (21).

$$\left[P_{\text{o}i} \leq 30\% P_{\text{o}i\_\text{rated}} \right] \rightarrow \left[\text{LP} = 1 \right]. \tag{25}$$

If a converter operates within a low-efficiency range, it can be switched OFF.

If more than one converter encounters a light load condition, the system will select the converter with the highest accumulated damage. This approach is intended to prevent decreased reliability in specific converters. Assuming there are w converters operating under light load conditions.

$$\begin{aligned} &\left[\text{AD}_{C\delta} = \text{AD}_{\max} \right. \\ &\qquad \left. = \max \left(\text{AD}_{C1}, \text{AD}_{C2} \cdots \text{AD}_{Cw} \right) \right] \rightarrow \left[C_\delta = 1 \right]. \end{aligned} \tag{26}$$

If more than one selected converter has relatively the same accumulated damage level, the proposed strategy will find the

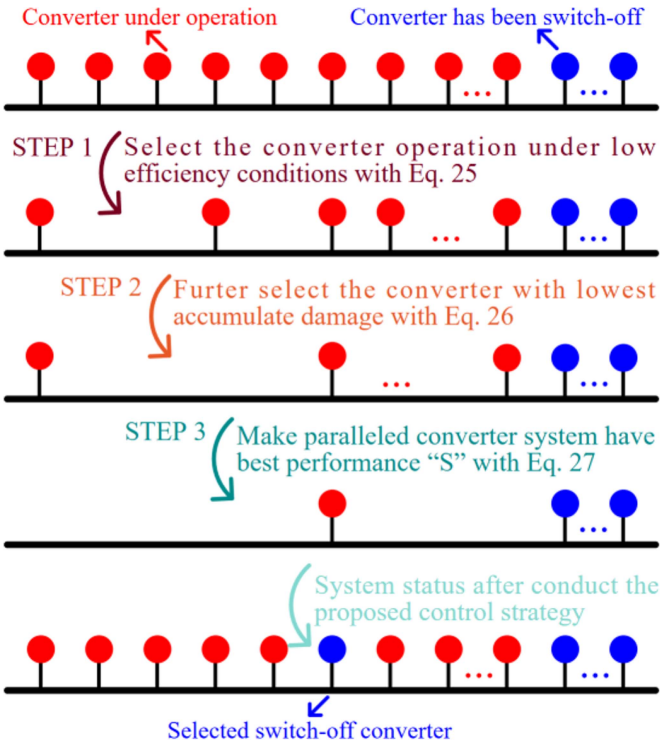

Fig. 4. Switch-OFF converter selected scheme of the proposed optimal selection strategy for operating converter combinations.

converter that after switching it OFF, the system can have the highest efficiency. Assuming x converters have the same relatively low accumulated damage level, the switch-OFF converter can be determined with

$$[S_\xi = S_{\max} = \max(S_1, S_2 \ldots S_x)] \rightarrow [C_\xi = 1] \tag{27}$$

where $S_1, S_2 \ldots S_x$ can be calculated with (15).

C_ξ is the selected switch-OFF converter. The switch-ON converter selected progress is shown in Fig. 4.

Once IGBTs are operated with extreme thermal stress, some converters should be switched ON to share the electrothermal stress. The switch-ON converter can be selected by considering the following aspects.

1) Reduce the switch time of the converter.
2) Choose the one that has the lowest accumulated damage to share the thermal stress.
3) Choose the one that can improve system efficiency as well as reliability after switching it ON with the help of the system's overall performance index S.

Defining HT = 1 to indicate the converter under the high thermal stress as shown in (25).

$$[T_{j\_i} \geq 90^\circ\mathrm{C}] \rightarrow [\mathrm{HT} = 1]. \tag{28}$$

To reduce the number of switch times, the switch-ON converter should be able to share the thermal stress, so as to bring the high-thermal stress converter into the desired operation range. It is assumed that among the n paralleled converters, m are currently active. The current of the converter after switching into the system can be calculated by

$$i_{oi} = \left(\frac{i_{\text{load}}}{m+1} + b_i^*\right) \Big/ (R_{\text{line}i} - 2a_i^*). \tag{29}$$

The switch-ON converter should operate in the desired thermal stress range after it is switched ON. In that case, the switch-in converter should meet the following condition:

$$\left[a_i\left(\frac{\frac{i_{\text{load}}}{m+1}+b_i^*}{R_{\text{line}i}-2a_i^*}\right)^2 + b_i\left(\frac{\frac{i_{\text{load}}}{m+1}+b_i^*}{R_{\text{line}i}-2a_i^*}\right) + c_i \leq \frac{T_{j\_\max}-T_a}{R_{\text{th}\_i}}\right] \rightarrow [C_i = 1] \tag{30}$$

If more than one converter meets the above condition, the switch-ON converter should be further selected according to the accumulated damage level of each converter. Assuming y converters meet the thermal need, the switch-ON converter can be further selected with

$$[\mathrm{AD}_{C\beta} = \mathrm{AD}_{\min} = \min(\mathrm{AD}_{C1}, \mathrm{AD}_{C2} \cdots \mathrm{AD}_{Cy})] \rightarrow [C_\beta = 1] \tag{31}$$

If more than one converter has the same accumulated damage level, the switch-ON converter is further selected according to the results of the dual-objective optimization function. Assuming that z converters have the same relatively low accumulated damage level, the switch-ON converter can be further selected by

$$S_i = a_i^*\left(\frac{\frac{i_{\text{Load}}}{m+1}+b_i^*}{R_{\text{line}i}-2a_i^*}\right)^2 + b_i^*\left(\frac{\frac{i_{\text{Load}}}{m+1}+b_i^*}{R_{\text{line}i}-2a_i^*}\right) + c_i^* \tag{32}$$

$$[S_\gamma = S_{\min} = \min(S_1, S_2 \ldots S_z)] \rightarrow [C_\gamma = 1] \tag{33}$$

where C_γ is the selected switch-ON converter. The switch-ON converter selected progress is shown in Fig. 5.

The proposed optimal selection strategy for operating converter combinations can change the status of the converter adaptively according to the system load condition and converter thermal condition. The optimal selection strategy for operating converter combinations will switch OFF the converter when the paralleled converter system is operated under light load conditions. By avoiding operation under light load conditions, the system efficiency can be increased. Meanwhile, the proposed control strategy can switch ON the converter once the temperature of the switching devices in other converters is high. By avoiding operation under high junction temperatures, the reliability of the paralleled converter system will be increased and the failure rate of the converter can be decreased. The system's efficiency and reliability can be improved simultaneously.

The proposed strategy requires communication of four floating-point variables $\mathrm{AD}_{\min}$, $\mathrm{AD}_{\max}$, $S_{\min}$, and $S_{\max}$, one int variable m and two Boolean variables LP and HT. With a communication frequency of 10 Hz, the required bandwidth is 1.62 kb/s. Long range is a wireless communication device that can work with low power, long distance, and low-bandwidth transmission [41]. It can transfer over distances of up to 15 km and offers a data rate of up to 50 kb/s, which satisfies the bandwidth and distance requirements of the proposed strategy.

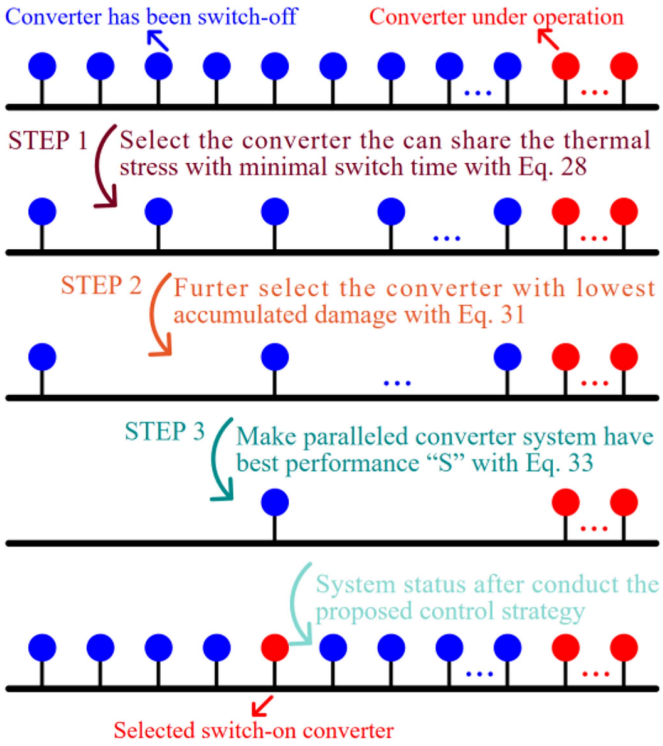

Fig. 5. Switch-ON converter selected scheme of the proposed optimal operation converter combination select strategy.

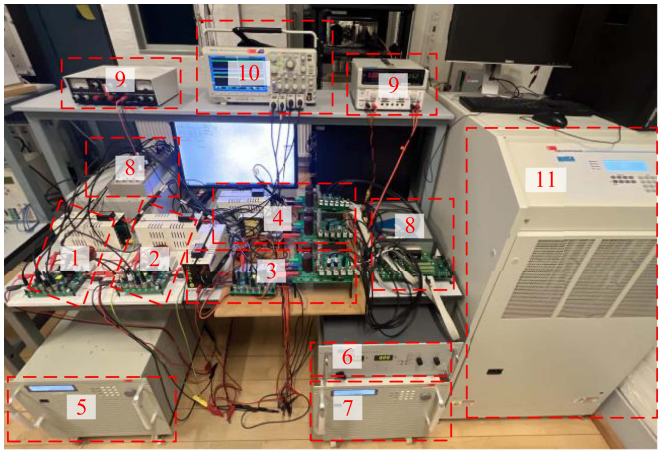

Fig. 6. Experiment platform with four paralleled converters. (1) Converter 1. (2) Converter 2. (3) Converter 3. (4) Converter 4. (5) Power source for converters 1 and 2. (6) Power source for converter 4. (7) Power source for converter 4. (8) Controller. (9) Auxiliary power supply. (10) Oscilloscope. (11) Constant power load.

IV. Experiment Verification

To verify the effectiveness of the proposed control strategy, an experimental prototype comprising four parallel branches connected to a constant power load is constructed, as shown in Fig. 6. The detailed information of the experimental prototype and key parameters are provided in Table I. The precise case temperature of the switching devices is measured using a thermal imager, enabling the subsequent calculation of the junction temperature based on (10).

TABLE I
System Parameters

Parameters	Values
Bus voltage	200 V
Converter 1 topology	Boost
Converter 2 topology	Boost
Converter 3 topology	H-bridge rectifier - boost
Converter 4 topology	Dual active bridge
Converter 1-rated power	500 W
Converter 2-rated power	1 kW
Converter 3-rated power	1.5 kW
Converter 4-rated power	2 kW
Converter 1 switching device	IKA15N65ET6
Converter 2 switching device	FGAF40N60UFTU
Converter 3 boost switching device	IKP28N65ES5
Converter 4 switching device/ H-bridge rectifier switching device	NGTB50N120FL2WG
Converter 1 power loss coefficients	a1 = 9.631, b1 = -20.37, c1 = 22.76
Converter 2 power loss coefficients	a2 = 5.732, b2 = -21.15, c2 = 46.75
Converter 3 power loss coefficients	a3 = 5.174, b3 = -20.79, c3 = 76.67
Converter 4 power loss coefficients	a4 = 3.981, b4 = -25.89, c4 = 107.67
Converter 1 IGBT thermal resistance	R_{th_jc} = 4.3K/W, R_{th_ca} = 3.39 K/W
Converter 2 IGBT thermal resistance	R_{th_jc} = 1.2K/W, R_{th_ca} = 2.14 K/W
Converter 3 H bridge rectifier IGBT thermal resistance	R_{th_jc} = 1.2 K/W, R_{th_ca} = 7.15 K/W
Converter 3 boost IGBT thermal resistance	R_{th_jc} = 1.2 K/W, R_{th_ca} = 3.39 K/W
Converter 4 IGBT thermal resistance	R_{th_jc} = 0.28 K/W, R_{th_ca} = 7.15 K/W
Cable resistance 1	0.2 Ω
Cable resistance 2	0.3 Ω
Cable resistance 3	0.4 Ω
Cable resistance 4	0.5 Ω
Switch frequency	$f_1 = f_2 = f_3 = f_4$ = 20 kHz

A. Proposed Power-Sharing Strategy Verification

Case 1: The proposed dual-objective optimal power-sharing control strategy compared with efficiency-prioritized control [22] and thermal sharing-prioritized control [33] under 60% rated load

The efficiency-prioritized control presented in [22] is first applied to the paralleled converters, after which the proposed control strategy is activated at the 10th second. Similarly, the thermal stress sharing-prioritized control proposed in [30] is first implemented for the paralleled converters, and the proposed optimal control strategy is subsequently enabled at the 10th second.

The experimental results are shown in Fig. 7. Specifically, Part 1 of Fig. 7 shows the power-sharing results and switching device thermal performance under the efficiency-prioritized control proposed in [22]. Part 2 presents the power-sharing results, switching device thermal performance, and weight coefficients under the proposed control strategy. Part 3 shows the power-sharing results and switching device thermal performance under thermal stress sharing-prioritized control proposed in [33]. Finally, Part 4 of Fig. 7 provides the results of the system's overall performance index considering efficiency and reliability under different control strategies.

A comparison between Part 1 and Part 2 of Fig. 7 reveals that the proposed control strategy achieves a lower thermal stress imbalance among the paralleled converters compared to the efficiency-prioritized control method in [22]. Specifically, the junction temperature difference is reduced from 20.6 °C to 7 °C, thereby mitigating excessive thermal stress on individual

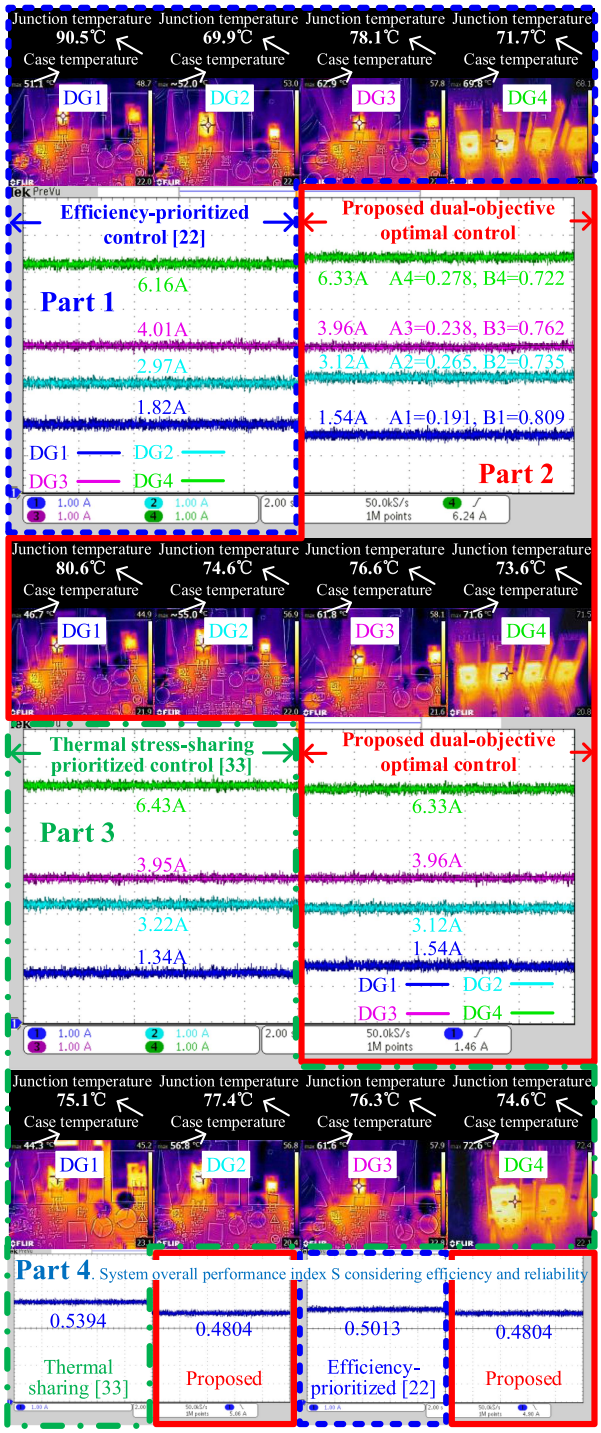

Fig. 7. Experiment results of power-sharing under efficiency-prioritized control [22], thermal stress sharing-prioritized control [33], and proposed dual objective optimal control strategy.

converters, which means under the proposed control, the branch with superior thermal performance undertakes more power. Furthermore, a comparison among Part 1, Part 2, and Part 3 of Fig. 7 demonstrates that the paralleled converter under the proposed control strategy has a minimum system overall performance index "S," indicating that the system achieves optimal performance in terms of both efficiency and reliability under the proposed control strategy.

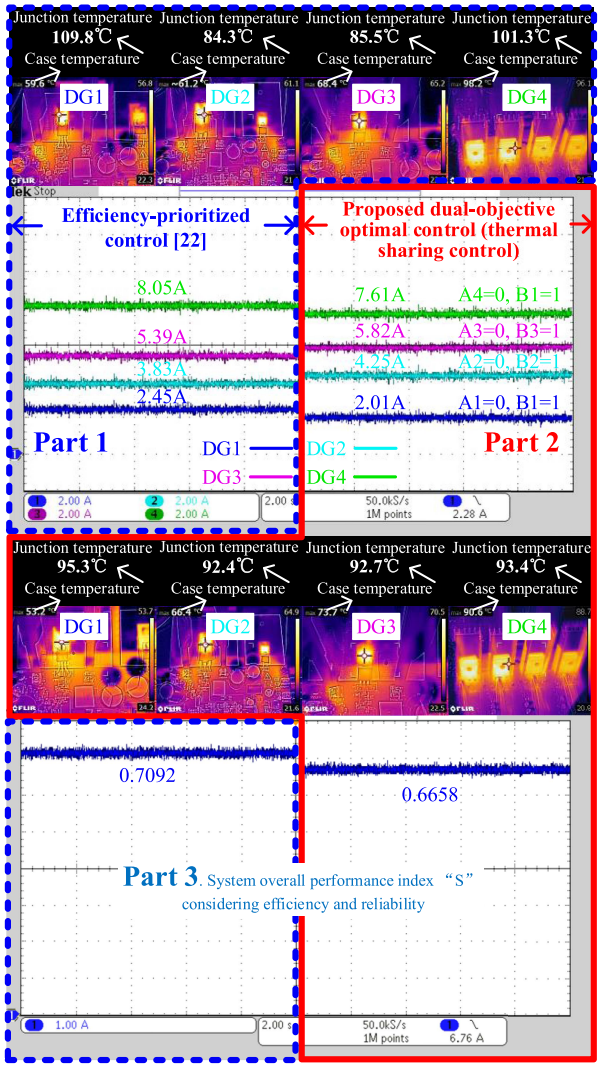

Fig. 8. Experiment results of power-sharing under efficiency-prioritized control [22] and proposed optimal control strategy.

Case 2: The proposed optimal power-sharing strategy compared with efficiency-prioritized control [22] under 80% rated load

In this case, the efficiency-prioritized control [22] is initially applied to the paralleled converters, and the proposed power-sharing control strategy is being activated at the 10th second. Due to the high thermal stress on each switching device, the weight coefficient of thermal stress B_i is set to 1. Consequently, the optimization objective of the proposed power-sharing strategy is to shift from a dual-objective approach to only thermal stress sharing.

The experimental results are shown in Fig. 8. Specifically, Part 1 of Fig. 8 shows the power-sharing results and switching device thermal performance under efficiency-prioritized control [22]. Part 2 presents the power-sharing results, switching device thermal performance, and weight coefficients under the proposed control strategy. Part 3 provides the system's overall performance index considering efficiency and reliability under different control strategies.

TABLE II
EXPERIMENT RESULTS UNDER 60% RATED LOAD AND 80% RATED LOAD WITH DIFFERENT CONTROL STRATEGIES

Load condition	60% rated load			80% rated load	
Control strategy	Efficiency-prioritized [22]	Thermal sharing [33]	Proposed control	Efficiency-prioritized [22]	Proposed control (thermal sharing)
T_j1/°C	90.5	75.1	80.6	109.8	95.3
T_j2/°C	69.9	77.4	74.6	84.3	92.4
T_j3/°C	78.1	76.3	76.6	85.5	92.7
T_j4/°C	71.7	74.6	73.6	101.3	93.4
Junction temperature difference/°C	20.6	2.8	7	25.5	2.9
System efficiency/%	91.63	91.02	91.27	90.24	89.79
Performance index "S"	0.5013	0.5394	0.4804√	0.7092	0.6658√

The red colored value in 60% rated load (the left one) is 0.4804; The red colored value in 80% rated load (the right one) is 0.6658.

As observed in Fig. 8, the paralleled converter operating under the proposed control strategy exhibits lower thermal stress imbalance. The temperature difference b among the switching devices within the paralleled converters is reduced from 25.5 °C to 2.9 °C. Additionally, the system's overall performance index "S" decreases from 0.7092 to 0.6658. These results indicate that the paralleled converter system achieves improved overall performance when employing the proposed power-sharing strategy.

The experiment results of power-sharing, thermal performance, and system performance index under 60% and 80% rated load with different control strategies are shown in Table II.

Case3: Bus voltage restoration capability verification

To evaluate the effectiveness of the proposed power-sharing strategy and its capability to restore bus voltage under sudden load variations, the load is switched from 3 to 1.5 kW at the 10th second. The corresponding power-sharing and bus voltage performance are shown in Fig. 9. As observed in Fig. 9, the proposed power-sharing strategy is activated effectively, ensuring proper system functionality and regulating the bus voltage to the desired value under sudden load reduction conditions.

B. Verification of the Proposed Optimal Selection Strategy for Operating Converter Combinations

Case 4: Proposed switched-OFF converter selection compared with switch-OFF strategy [18]: Load decrease from 1.5 kW to 1.2 kW to 0.6 kW

To validate the effectiveness of the proposed optimal selection strategy for operating converter combinations, the load is reduced from 1.5 to 1.2 kW and subsequently to 0.6 kW, representing system operation under light load conditions. To ensure a clear differentiation of the experimental results, it is assumed that all four paralleled converters have the same accumulated damage

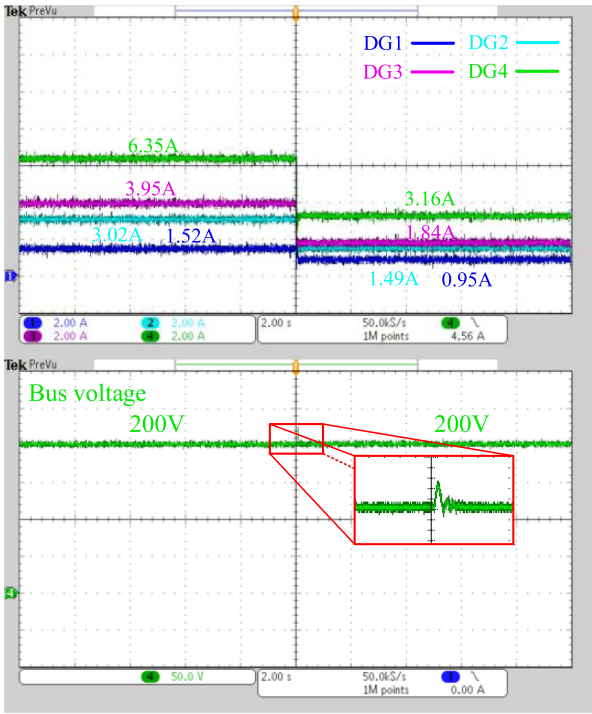

Fig. 9. Experiment results of the proposed dual-objective optimal control strategy and bus voltage under sudden load decrease.

level in Case 4 and Case 5. The converter switches-OFF selection results under load decrease conditions, comparing the proposed strategy with the strategy presented in [18], are illustrated in Fig. 10.

It can be seen from Fig. 10 that with the load decreases, the system has different operating converter combinations. Under each load condition, different selected operating converter combination results in a distinct overall performance index, as shown in Fig. 11

Compared with the switch-OFF strategy proposed in [18], the paralleled converter system under the proposed strategy achieves a lower overall performance index value. It indicates the improved system performance, considering both efficiency and reliability.

Case 5: Proposed switched-ON converter selection compared with switch-ON strategy [18] : Load increase from 0.3 kW to 1.2 kW to 2.4 kW

To validate the effectiveness of the proposed optimal selection strategy for operating converter combinations, the load increased from 0.3 to 1.2 kW and subsequently to 2.4 kW. The converter switches-ON selection results under the proposed strategy and the strategy presented in [18] are shown in Fig. 12. The corresponding system overall performance index "S" are shown in Fig. 13.

As observed in Fig. 13, the paralleled converter system operating under the proposed strategy achieves a lower overall performance index compared to the strategy proposed in [18]. It indicates that the proposed strategy enables paralleled converters to achieve superior overall system performance.

The improved performance and differing selection results observed under Case 4 (load decrease) and Case 5 (load increase)

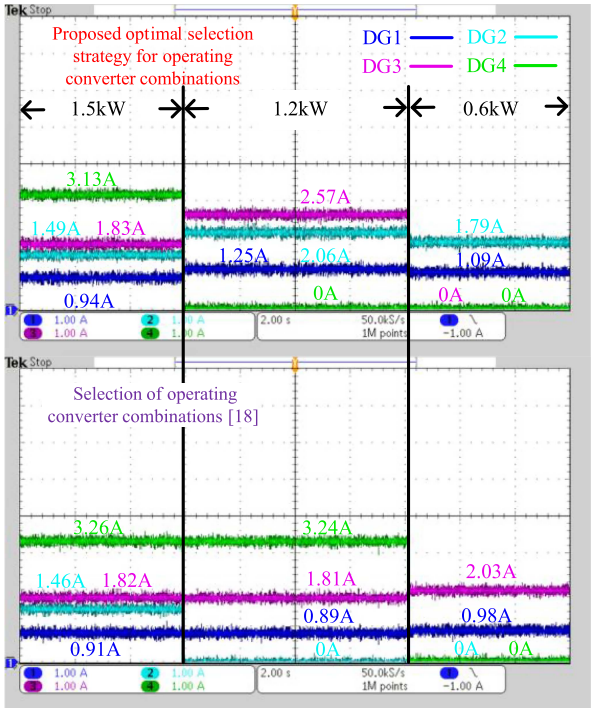

Fig. 10. Paralleled converters' operation status under the proposed optimal selection strategy for operating converter combinations and the selection strategy proposed in [18].

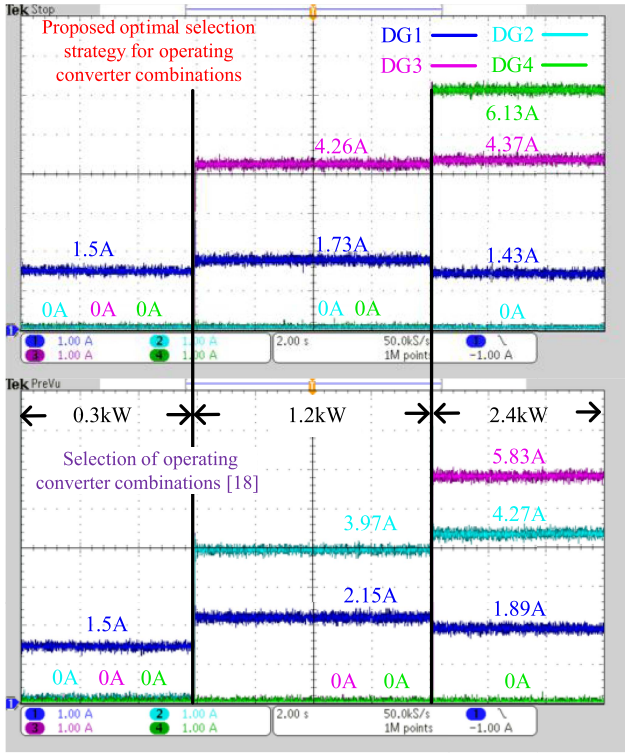

Fig. 12. Paralleled converters' operation status under the proposed optimal selection strategy for operating converter combinations and the selection strategy proposed in [18].

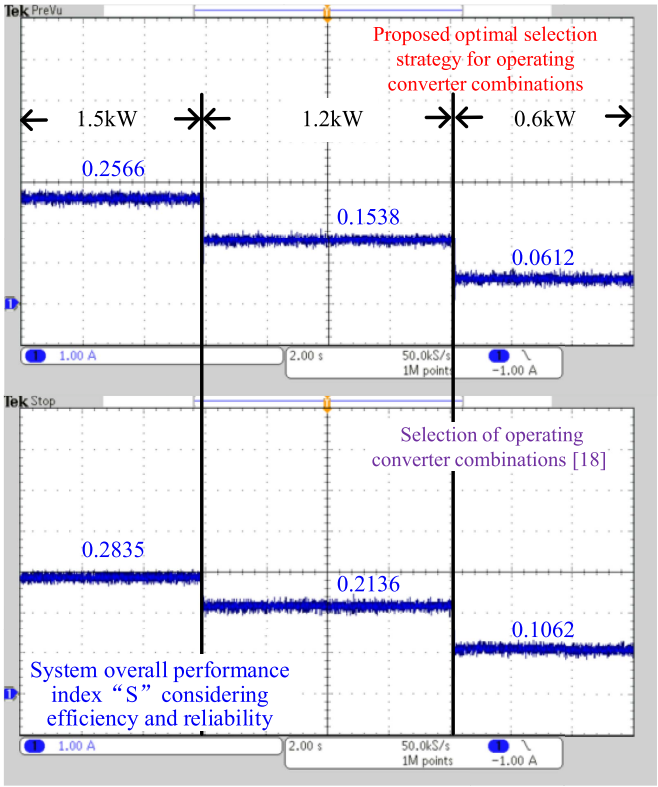

Fig. 11. System overall performance index "S" under the proposed optimal selection strategy for operating converter combinations and the selection strategy proposed in [18].

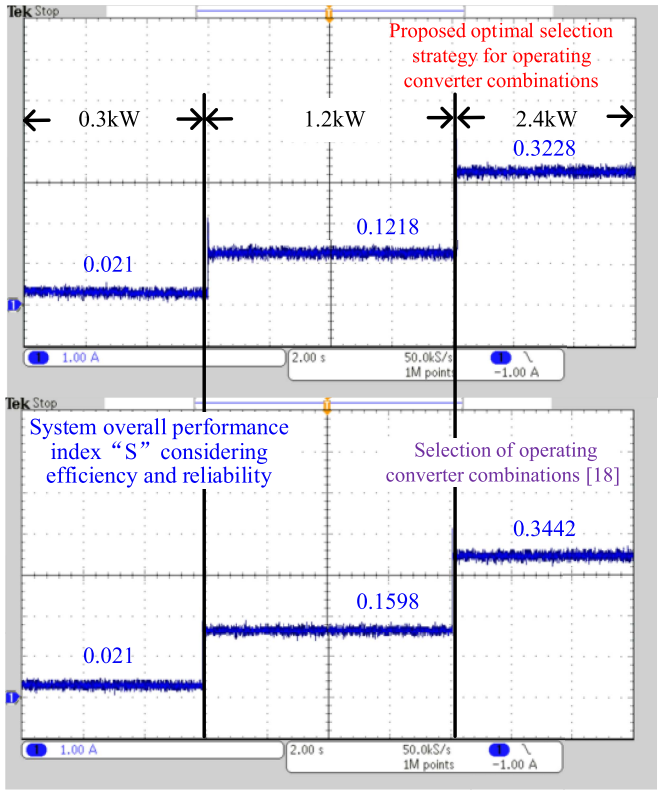

Fig. 13. System overall performance index "S" under the proposed optimal selection strategy for operating converter combinations and the selection strategy proposed in [18].

can be attributed to the fact that the proposed strategy considers not only efficiency but also the thermal stress of the switching devices in the selection progress, leading to a more balanced and optimized system operation.

V. Conclusion

This article presents an optimal operation strategy to improve efficiency and reliability for paralleled converters in offshore dc microgrids. By integrating a dual-objective optimization model and an active weight coefficient-based adaptive power-sharing mechanism, the proposed method can dynamically balance power distribution and thermal stress among paralleled converters. Furthermore, a decentralized dispatch scheme for the optimal selection strategy of operating converter combinations is introduced to improve performance within a wide load range. Experimental results validate the effectiveness of the proposed approach, demonstrating significant reductions in thermal stress imbalance among switching devices in paralleled converters and improvements in overall system efficiency. The proposed strategy effectively optimizes the overall performance considering efficiency and reliability, which provides a practical and scalable solution for enhancing the system performance of the offshore microgrid.

References

[1] L. Zhou et al., "Virtual positive-damping reshaped impedance stability control method for the offshore MVDC system," *IEEE Trans. Power Electron.*, vol. 34, no. 5, pp. 4951–4966, May 2019.

[2] P. Catalán, Y. Wang, J. Arza, and Z. Chen, "A comprehensive overview of power converter applied in high-power wind turbine: Key challenges and potential solutions," *IEEE Trans. Power Electron.*, vol. 38, no. 5, pp. 6169–6195, May 2023.

[3] J. Wang, W. Huang, N. Tai, M. Yu, R. Li, and C. Li, "An adaptive inertia transferring control scheme for interconnected offshore-platform microgrids," *IEEE Trans. Power Del.*, vol. 39, no. 1, pp. 591–600, Feb. 2024.

[4] X. Zhu, Y. Wang, and Z. Chen, "New perspectives on zero emission marine transportation: Offshore hybrid energy refueling system," in *Proc. IEEE Energy Convers. Congr. Expo.*, 2023, pp. 99–104.

[5] P. Huang and L. Vanfretti, "Multi-tuned narrowband damping for suppressing MMC high-frequency oscillations," *IEEE Trans. Power Del.*, vol. 38, no. 6, pp. 3804–3819, Dec. 2023.

[6] M. Mosayebi, S. M. Sadeghzadeh, M. Gheisarnejad, and M. H. Khooban, "Intelligent and fast model-free sliding mode control for shipboard dc microgrids," *IEEE Trans. Transp. Electrific.*, vol. 7, no. 3, pp. 1662–1671, Sep. 2021.

[7] N. Hou and Y. Li, "Communication-free power management strategy for the multiple DAB-based energy storage system in islanded dc microgrid," *IEEE Trans. Power Electron.*, vol. 36, no. 4, pp. 4828–4838, Apr. 2021.

[8] P. Huang and L. Vanfretti, "Adaptive damping control of MMC to suppress high-frequency resonance," *IEEE Trans. Ind. Appl.*, vol. 59, no. 6, pp. 7224–7237, Nov./Dec. 2023.

[9] X. Yu, A. M. Khambadkone, H. Wang, and S. T. S. Terence, "Control of parallel-connected power converters for low-voltage microgrid—Part I: A hybrid control architecture," *IEEE Trans. Power Electron.*, vol. 25, no. 12, pp. 2962–2970, Dec. 2010.

[10] W. Yuan, Y. Wang, X. Ge, X. Hou, and H. Han, "A unified distributed control strategy for hybrid cascaded-parallel microgrid," *IEEE Trans. Energy Convers.*, vol. 34, no. 4, pp. 2029–2040, Dec. 2019.

[11] Q. Zhao, K. Liao, J. Yang, Z. He, and Y. Xu, "Aging rate equalization strategy for battery energy storage systems in microgrids," *IEEE Trans. Smart Grid*, vol. 15, no. 1, pp. 136–148, Jan. 2024.

[12] Y. Wang, D. Liu, Z. Chen, and P. Liu, "A hierarchical control strategy of microgrids toward reliability enhancement," in *Proc. Int. Conf. Smart Grid*, 2018, pp. 123–128.

[13] Y. Wang, D. Liu, P. Liu, F. Deng, D. Zhou, and Z. Chen, "Lifetime-oriented droop control strategy for ac islanded microgrids," *IEEE Trans. Ind. Appl.*, vol. 55, no. 3, pp. 3252–3263, May/Jun. 2019.

[14] X. Zhu, Y. Wang, C. Liu, N. Hou, Y. Li, and Z. Chen, "A dual-level optimal control strategy for offshore microgrid considering efficiency and operation cost in wide load range," *IEEE Trans. Power Electron.*, vol. 39, no. 6, pp. 6734–6744, Jun. 2024.

[15] T. Hirose, M. Takasaki, and Y. Ishizuka, "A power efficiency improvement technique for a bidirectional dual active bridge dc–dc converter at light load," *IEEE Trans. Ind. Appl.*, vol. 50, no. 6, pp. 4047–4055, Nov./Dec. 2014.

[16] P. Bartal and I. Nagy, "Game theoretic approach for achieving optimum overall efficiency in dc/dc converters," *IEEE Trans. Ind. Electron.*, vol. 61, no. 7, pp. 3202–3209, Jul. 2014.

[17] H. Zhang, J. Zhou, Q. Sun, J. M. Guerrero, and D. Ma, "Data-driven control for interlinked ac/dc microgrids via model-free adaptive control and dual-droop control," *IEEE Trans. Smart Grid*, vol. 8, no. 2, pp. 557–571, Mar. 2017.

[18] N. A. Ashtiani, A. Sheykhi, and S. A. Khajehoddin, "Modified droop strategy for wide load range efficiency improvement of parallel inverter systems," *IEEE Trans. Power Electron.*, vol. 37, no. 7, pp. 8433–8446, Jul. 2022.

[19] S. Wang, J. Liu, Z. Liu, T. Wu, and B. Liu, "Efficiency-based optimization of steady-state operating points for parallel source converters in standalone power system," in *Proc. IEEE 8th Int. Power Electron. Motion Control Conf.*, 2016, pp. 163–170.

[20] J. He and Y. W. Li, "Generalized closed-loop control schemes with embedded virtual impedances for voltage source converters with LC or LCL filters," *IEEE Trans. Power Electron.*, vol. 27, no. 4, pp. 1850–1861, Apr. 2012.

[21] J. He and Y. W. Li, "Analysis, design, and implementation of virtual impedance for power electronics interfaced distributed generation," *IEEE Trans. Ind. Appl.*, vol. 47, no. 6, pp. 2525–2538, Nov./Dec. 2011.

[22] W. Yuan, Y. Wang, D. Liu, F. Deng, and Z. Chen, "Efficiency-prioritized droop control strategy of ac microgrid," *IEEE J. Emerg. Sel. Top. Power Electron.*, vol. 9, no. 3, pp. 2936–2950, Jun. 2021.

[23] M. Andresen, V. Raveendran, G. Buticchi, and M. Liserre, "Lifetime-based power routing in parallel converters for smart transformer application," *IEEE Trans. Ind. Electron.*, vol. 65, no. 2, pp. 1675–1684, Feb. 2018.

[24] H. Liu, K. Ma, Z. Qin, P. C. Loh, and F. Blaabjerg, "Lifetime estimation of MMC for offshore wind power HVDC application," *IEEE J. Emerg. Sel. Top. Power Electron.*, vol. 4, no. 2, pp. 504–511, Jun. 2016.

[25] G. Buticchi, M. Andresen, M. Wutti, and M. Liserre, "Lifetime-based power routing of a quadruple active bridge dc/dc converter," *IEEE Trans. Power Electron.*, vol. 32, no. 11, pp. 8892–8903, Nov. 2017.

[26] A. Marquez et al., "Power devices aging equalization of interleaved dc–dc boost converters via power routing," *IEEE J. Emerg. Sel. Top. Ind. Electron.*, vol. 1, no. 1, pp. 91–101, Jul. 2020.

[27] V. Raveendran, M. Andresen, and M. Liserre, "Improving onboard converter reliability for more electric aircraft with lifetime-based control," *IEEE Trans. Ind. Electron.*, vol. 66, no. 7, pp. 5787–5796, Jul. 2019.

[28] J. Wei et al., "Behaviour and mechanisms of molecular vibrations induced by a pulsed voltage in a silicone elastomer used for device encapsulation," *High Voltage*, vol. 8, no. 5, pp. 1020–1029, Aug. 2023.

[29] X. Wei et al., "A robust online junction temperature calibration method for power semiconductors in traction inverter application," *IEEE Trans. Transp. Electrific.*, vol. 11, no. 2, pp. 6602–6614, Apr. 2025, doi: 10.1109/TTE.2024.3512941.

[30] I. F. Kovačević, U. Drofenik, and J. W. Kolar, "New physical model for lifetime estimation of power modules," in *Proc. Int. Power Electron. Conf.*, 2010, pp. 2106–2114.

[31] A. Arya, A. Chanekar, P. Deshmukh, A. Verma, and S. Anand, "Accurate online junction temperature estimation of IGBT using inflection point based updated I–V characteristics," *IEEE Trans. Power Electron.*, vol. 36, no. 9, pp. 9826–9836, Sep. 2021.

[32] S. Yang, A. Bryant, P. Mawby, D. Xiang, L. Ran, and P. Tavner, "An industry-based survey of reliability in power electronic converters," *IEEE Trans. Ind. Appl.*, vol. 47, no. 3, pp. 1441–1451, May/Jun. 2011.

[33] V. Raveendran, M. Andresen, G. Buticchi, and M. Liserre, "Thermal stress based power routing of smart transformer with CHB and DAB converters," *IEEE Trans. Power Electron.*, vol. 35, no. 4, pp. 4205–4215, Apr. 2020.

[34] M. Andresen, K. Ma, G. Buticchi, J. Falck, F. Blaabjerg, and M. Liserre, "Junction temperature control for more reliable power electronics," *IEEE Trans. Power Electron.*, vol. 33, no. 1, pp. 765–776, Jan. 2018.

[35] Y. Wang, P. Liu, D. Liu, F. Deng, and Z. Chen, "Enhanced hierarchical control framework of microgrids with efficiency improvement and thermal management," *IEEE Trans. Energy Convers.*, vol. 36, no. 1, pp. 11–22, Mar. 2021.

[36] K. Ma, M. Liserre, F. Blaabjerg, and T. Kerekes, "Thermal loading and lifetime estimation for power device considering mission profiles in wind power converter," *IEEE Trans. Power Electron.*, vol. 30, no. 2, pp. 590–602, Feb. 2015.

[37] *IGBT Modules Technical Information*, IKA15N65ET6, Datasheet, Infineon Technologies AG, Munich, Germany, 2021.
[38] *IGBT Modules Technical Information*, FGAF40N60UFTU, Datasheet, Onsemi, Colorado, USA, 2004.
[39] *IGBT Modules Technical Information*, IKP28N65ES5, Datasheet, Infineon, Munich, Germany, 2019.
[40] *IGBT Modules Technical Information*, NGTB50N120FL2WG, Datasheet, Onsemi, Denver, Colorado, USA, 2015.
[41] H.-C. Lee and K.-H. Ke, "Monitoring of large-area IoT sensors using a LoRa wireless mesh network system: Design and evaluation," *IEEE Trans. Instrum. Meas.*, vol. 67, no. 9, pp. 2177–2187, Sep. 2018.

Xiangchen Zhu (Student Member, IEEE) received the B.S. degree in electrical engineering and automation from the Shanghai University of Engineering Science, Shanghai, China, in 2017, and the master's degree in mechanical electronics with joint supervision of Shanghai University of Electrical Power and Shanghai University of Engineering Science, Shanghai, China, in 2021. He is currently working toward the Ph.D. degree in electrical engineering with the Department of Energy, Aalborg University, Aalborg, Denmark.

From July 2023 to January 2024, he was a visiting scholar with the Electronic and Intelligent Grid Research Lab of the Department of Electrical and Computer Engineering, University of Alberta, Edmonton, AB, Canada. His research interests include the optimal operation of ocean energy, offshore microgrid control, power electronic system reliability enhancement, and data-based intelligent power electronic control.

Pengxiang Huang (Member, IEEE) received the B.S. degree from the Shanghai University of Electric Power, Shanghai, China, in 2015, the M.S. degree from George Washington University, Washington, DC, USA, in 2018, and the Ph.D. degree from Rensselaer Polytechnic Institute, Troy, NY, USA, in 2023, all in electrical engineering.

He is currently a Research Engineer with the National Renewable Energy Laboratory, Golden, CO, USA. His research interests include renewable energy integration, dc transmission and distribution systems, flexible ac transmission systems, and data center power systems.

Hanwen Zhang (Graduate Student Member, IEEE) received the B.Eng. and M.Sc. degrees in electrical engineering from Northeast Electric Power University, Jilin City, China, in 2017 and 2020, respectively, and the Ph.D. degree in electrical engineering from Aalborg University, Aalborg, Denmark, in 2025.

He is currently a Research Associate with the Department of Electronic and Electrical Engineering, University of Bath, Bath, U.K. In 2018, he was a visiting student with the School of Engineering, Cardiff University. He was invited as a guest Ph.D. student with the Department of Industrial Engineering, University of Rome "Tor Vergata," Rome, Italy, in 2023, and with the Department of Engineering Technology and Didactics, Technical University of Denmark, in 2024. From 2022 to 2025, he was a Ph.D. student researcher on the European DEMOnstration Power Plant project under the EUROfusion Consortium, as part of the European Union's Horizon Europe Framework Programme. His research interests include dc microgrids, multiport dc–dc converters, dc circuit breakers, and power systems for nuclear fusion applications.

Yanbo Wang (Senior Member, IEEE) received the Ph.D. degree in electrical engineering from the Department of Energy Technology, Aalborg University, Aalborg, Denmark, in 2017.

He is currently an Associate Professor with the Department of Energy Technology, Aalborg University. He is the vice leader of Wind Power System Research program at the Department of Energy Technology, Aalborg University. From June to October of 2016, he was a visiting scholar with the Power System Research Group of the Department of Electrical and Computer Engineering, University of Manitoba, Winnipeg, MB, Canada. His research interests include distributed power generation systems, wind power systems, microgrids, and power electronic-dominated power systems.

Ruizhi Wei (Graduate Student Member, IEEE) received the B.S. degree in electrical engineering from the Nanjing University of Science and Technology, Nanjing, China, in 2018, and the M.S. degree in electrical engineering from the Harbin Institute of Technology, Harbin, China, in 2020. He is currently working toward the Ph.D. degree in electrical engineering with the Department of Electrical and Computer Engineering, University of Alberta, Edmonton, AB, Canada.

His current research interests include control and optimization of bidirectional dc–dc converters and their applications.

Ning Wang (Student Member, IEEE) received the B.Eng. degree in electrical engineering from Jilin University, Changchun, China, in 2015, and M.Sc. degree in electrical engineering from Xi'an Jiaotong University, Xi'an, China, in 2018. He is currently working toward the Ph.D. degree in electrical engineering with Aalborg University, Aalborg, Denmark.

His research interests include dc–dc converters, advanced control algorithms, and renewable energy systems.

Yunwei Li (Fellow, IEEE) received the B.Sc. degree in electrical engineering from Tianjin University, Tianjin, China, in 2002, and the Ph.D. degree in electrical engineering from Nanyang Technological University, Singapore, in 2006.

In 2005, he was a Visiting Scholar with Aalborg University, Aalborg, Denmark. From 2006 to 2007, he was a Postdoctoral Research Fellow with Ryerson University. In 2007, he was also with Rockwell Automation Canada before he joined the University of Alberta in the same year. Since then, he has been with the University of Alberta, where he is currently a Professor and the Acting Department Chair. His research interests include distributed generation, microgrid, renewable energy, high power converters, and electric motor drives.

Dr. Li is currently the Editor-in-Chief of IEEE TRANSACTIONS ON POWER ELECTRONICS LETTERS. Before that, he was an Associate Editor for the IEEE TRANSACTIONS ON POWER ELECTRONICS, IEEE TRANSACTIONS ON INDUSTRIAL ELECTRONICS, IEEE TRANSACTIONS ON SMART GRID, and IEEE JOURNAL OF EMERGING AND SELECTED TOPICS IN POWER ELECTRONICS. In 2020, he was the General Chair for the IEEE Energy Conversion Congress of Exposition. He is the AdCom Member at Large for IEEE Power Electronics Society 2021–2023. He is recognized as a Highly Cited Researcher by the Web of Science Group. He was the recipient of the Richard M. Bass Outstanding Young Power Electronics Engineer Award from the IEEE Power Electronics Society in 2013.

Zhe Chen (Fellow, IEEE) received the B.Eng. and M.Sc. degrees in electrical engineering from Northeast China Institute of Electric Power Engineering, Jilin City, China, and the Ph.D. degree in electrical engineering from the University of Durham, Durham, U.K.

He is currently a full Professor with the Department of Energy Technology, Aalborg University, Aalborg, Denmark. He is also the Leader of the Wind Power System Research program at the Department of Energy Technology, Aalborg University and the Danish Principal Investigator for Wind Energy of Sino-Danish Centre for Education and Research. His research interests include power systems, power electronics and electric machines, and wind energy and modern power systems.

Dr. Chen is an Associate Editor for IEEE TRANSACTIONS ON POWER ELECTRONICS, a Member of Editorial Boards for many international journals, a Fellow of the Institution of Engineering and Technology (London, U.K.), and a Chartered Engineer in the U.K.